Progress in Natural Science: Materials International 30 (2020) 337–342

Contents lists available at ScienceDirect

Progress in Natural Science: Materials International

journal homepage: www.elsevier.com/locate/pnsmi

Original Research

Self-rolled TiO_2 microscroll/graphene composite for electrochemical dopamine sensing

Fei Ma[a], Bin Yang[b], Zhiwei Zhang[a], Jilie Kong[b], Gaoshan Huang[a], Yongfeng Mei[a,*]

[a] *Department of Materials Science, Fudan University, Shanghai, 200433, China*
[b] *Department of Chemistry, Fudan University, Shanghai, 200433, China*

ARTICLE INFO

Keywords:
Electrochemical sensor
Dopamine sensor
Self-rolling
Microscroll
3D nanostructures

ABSTRACT

Dopamine is an important neurotransmitter, and nonenzyme electrochemical sensor of dopamine detection based on highly active material is urgently demanded. In this work, an electrochemical sensor with high sensitivity and selectivity based on self-rolled TiO_2 microscroll/graphene composite was developed and validated for dopamine sensing. The device exhibited a superior performance for dopamine detection with a detection limit of 4.25×10^{-9} mol L^{-1}, and in the dopamine concentration range of 0.06–90 μmol L^{-1}, the oxidation currents increased linearly with the concentration. The remarkable performance enhancement was mainly ascribed to the increased surface area due to the porous surface of the TiO_2 nanomembrane and highly conductive graphene therein. In addition, we have demonstrated that the sensor could be effectively used on detecting dopamine concentrations in urine samples. Our work demonstrates that the current microscroll-based device is promising in the field of real-time health monitoring for future human community.

1. Introduction

People's ideology and physiological behaviors are closely related to neurotransmitters transmission. Neurological diseases such as Alzheimer's, Parkinson's, schizophrenia, and depression are often aroused by neurological disorders [1]. Abnormal concentration levels of neurotransmitters like dopamine (DA) always cause diseases, and therefore sensitive detection of DA and other neurotransmitters is essential for the diagnosis of neurological diseases [2]. In the past few decades, the electrochemical methods have been recognized as a simple and effective approach for detection of biological matrices, e.g., sweat, urine, serum, and cell culture media [3–8]. However, selectivity and sensitivity of DA detection was restricted in the presence of interfering species. Therefore, electrode with large surface area was always involved which results in fast electron transfer rate, ensuring the sensitivity of electrochemical sensor [8]. Recently, rolled-up technology have attracted much attention because it allows convenient self-assembly of 2D nanomembranes into 3D structures at nanoscale [9]. By this means, large surface area and reduced space occupancy can be realized simultaneously. Rolled-up nanomembranes could build up a mixed electron/ion conductive network as the supporting layer which serves as a continuous transport pathway for electrons, and the hollow space provides fast transportation channel for redox reaction, which should be meaningful for electrochemical sensing [10–12]. Moreover, in such structures, materials in the form of flexible nanomembrane can sustain against stress cracking in electrochemical process and greatly enhance the stability [13]. In the past years, applications of rolled-up 3D structures in the fields of radio-frequency integrated circuits [14], energy storage devices [15], and cellular cargo delivery [16] have already been explored with promoted performance. Herein, considering above-mentioned advantages, we expect that rolled-up nanomembrane-based electrochemical sensor for neurotransmitters (e.g., DA) should have excellent performance as well.

As for the active materials of the electrochemical sensors, titanium dioxide (TiO_2) is widely used because of its excellent biocompatibility and catalytic properties. It has been found that TiO_2 micro-/nano-structures could facilitate the direct electron transfer process between analytes and the electrode surface due to its large surface area [17,18]. Various TiO_2 structures like nanotubes, nanorods, nanobelts, nanowires, microspheres, and mesoporous fibers have been synthesized and utilized in electrochemical field [19–27]. High specific surface area and more reactive sites for redox reaction have been achieved in these micro-/nano-structures but the relatively large resistivity of TiO_2 may influence the electron transfer process [28]. Further improvement in the electrochemical performance of the TiO_2 micro-/nano-structures should be realized if the conductivity of the electrode can be increased [29]. Thus, incorporating materials with high electron conductivity is a good option. As we know, graphene has two dimensional honeycomb-

---

[*] Corresponding author.
E-mail address: yfm@fudan.edu.cn (Y. Mei).

https://doi.org/10.1016/j.pnsc.2020.02.008
Received 17 September 2019; Received in revised form 27 February 2020; Accepted 28 February 2020
Available online 12 June 2020
1002-0071/ © 2020 Chinese Materials Research Society. Published by Elsevier B.V. This is an open access article under the CC BY-NC-ND license (http://creativecommons.org/licenses/BY-NC-ND/4.0/).

like lattice and own atomic layer thickness [30]. The unique structure leads to exceptional physical properties, such as high electron conductivity and surface effects [31,32]. Previous researches [33–37] have already produced graphene-based electrodes with fast response time and good biological compatibility [38]. We therefore believe that the combination of rolled-up TiO_2 structures and graphene may further improve the performance of the obtained electrochemical sensing device.

In this work, an electrochemical sensing platform was developed for DA sensing by using rolled-up TiO_2 microscrolls decorated with graphene. Here, TiO_2 porous nanomembranes with high specific surface area were firstly obtained by atomic layer deposition (ALD) and then hollow TiO_2 microscrolls were prepared by a sonication-induced rolling process. After that graphene was dispersed and decorated on the surface of TiO_2 microscrolls, the obtained TiO_2 microscroll/graphene composite electrode exhibited excellent performance for DA sensing. The kinetic process of DA catalytic reaction on the electrode was studied. According to previous research, graphene and TiO_2 are considered as non-toxic biocompatible materials, and can be used for *in vivo* monitoring [39]. Thus, we propose that the current platform based on TiO_2 microscroll/graphene composite is quite promising for *in vivo* applications.

2. Experimental details

2.1. Preparation of rolled-up TiO_2 microscroll/graphene composite

Fig. 1a demonstrates the fabrication process of TiO_2 microscroll/graphene composite. Firstly, TiO_2 porous nanomembrane was obtained by a template-assisted ALD process [40]. In this process, TiO_2 nanomembrane (thickness: 40 nm) was deposited on the porous polymer template, followed by a high temperature annealing process in O_2 where the polymer template was removed. The TiO_2 3D interconnected structure duplicated the geometry of the original template was then crushed to produce a large amount of TiO_2 nanomembranes (Fig. 1a–I). More details can be found in our previous work [40]. The obtained TiO_2 nanomembranes were then immersed in ethanol under 20 kHz sonication for 1 min to roll the nanomembranes into microscrolls (Fig. 1a–II). TiO_2 microscroll/graphene composite was fabricated by mixing TiO_2 microscroll and graphene powder (weight ratio = 2:1) in ethanol (Fig. 1a–III, see also section 2.2).

2.2. Construction of electrochemical sensor

Firstly, the surface of glassy carbon electrode (GCE) was polished successively with 3 finer-grade aqueous alumina slurries (1.0, 0.3, and 0.05 μm grain sizes) on chamois leather. Then the electrode was washed with HNO_3 (50% in volume), ethyl alcohol, and deionized water successively. For the preparation of TiO_2 microscroll/graphene electrode, 2 mg TiO_2 microscroll, 1 mg graphene powder, and 0.05 mL 0.03 wt% nafion (in ethanol) was dispersed into 20 mL ethanol. The mixture was sonicated (20 kHz) for 1 min to achieve a stable and homogeneous suspension. 4.0 μL modification solution was then dropped onto the surface of the electrode and the electrode was dried at room temperature for 2 h. For comparison, TiO_2 microscroll electrode, TiO_2 nanomembrane electrode, and graphene electrode were also prepared with a

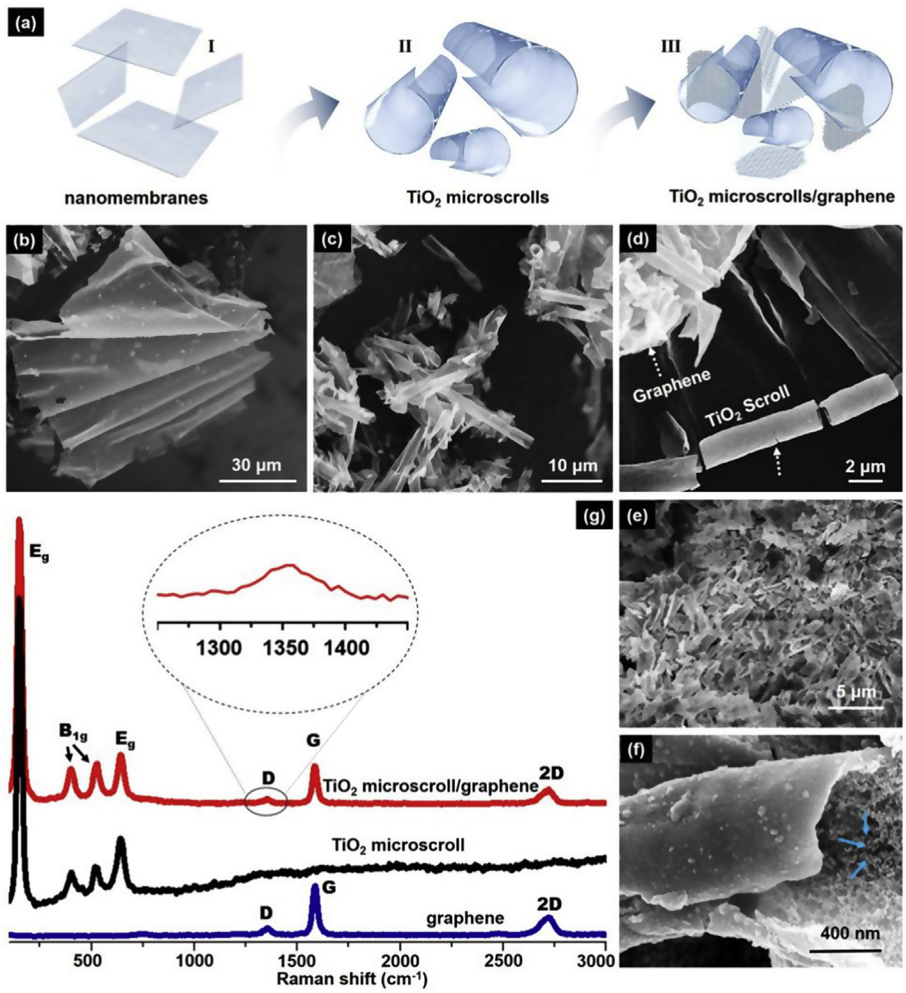

Fig. 1. Fabrication of microscrolls and their application in DA sensing. a) Schematic of the fabrication process. b) SEM images of TiO_2 nanomembranes, c) microscrolls, and d) microscroll/graphene composite. e) SEM image of TiO_2 microscroll/graphene composite on electrode surface. f) SEM image of TiO_2 microscroll hollow structure with porous inner surface. The blue arrows indicate the porous structure. g) Raman spectra of TiO_2 microscroll, graphene, and TiO_2 microscroll/graphene composite. The inset is the enlarged D peak. (For interpretation of the references to colour in this figure legend, the reader is referred to the Web version of this article.)

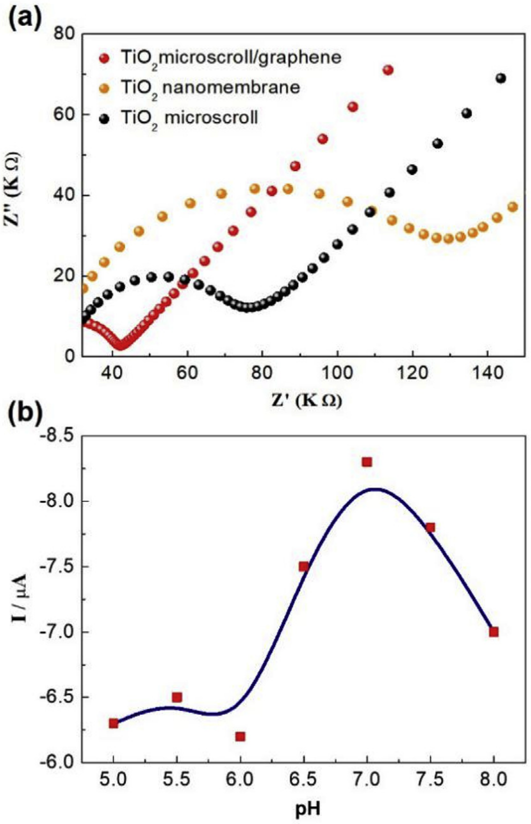

Fig. 2. a) EIS results of TiO_2 microscrolls, TiO_2 microscroll/graphene composite, and TiO_2 nanomembrane. b) Evolution of I_{pa} as a function of the pH of analyte solution containing 1 mol L^{-1} Tris-HCl and 0.2 μmol L^{-1}DA.

similar procedure.

2.3. Microstructural characterizations

The morphologies of samples were investigated by using scanning electron microscopy (SEM, JEOL JSM6701F). The structural properties of the samples were characterized by Raman spectrometer (LabRAM HR Evolution, Horiba Jobin Yvon) with a 532 nm laser as the excitation source.

2.4. Electrochemical characterizations

Differential pulse voltammetry (DPV), cyclic voltammetry (CV), and electrochemical impedance spectroscopy (EIS) of the samples were performed on electrochemical workstations (Metrohm Autolab PGSTAT302 N and CHI 660D). In the DPV and CV experiments, the electrode was placed in a mixed buffer solution which consisted of DA and 1 mol L^{-1} Tris-HCl buffer solution. The DPV measurement was carried out in the voltage range of 0–0.4 V, with different scan rates. The EIS characterization was carried out in a mixed solution of 0.05 mol L^{-1} $K_3[Fe(CN)_6]/K_4[Fe(CN)_6]$ and 0.5 mol L^{-1} KCl. The frequency range of EIS characterization is 10^{-1}–10^5 Hz, and the alternating voltage is 5 mV.

3. Results and discussions

3.1. Structural properties

The morphologies of TiO_2 nanomembranes, TiO_2 microscrolls, and TiO_2 microscroll/graphene composite were characterized by SEM. The TiO_2 nanomembranes obtained after removal of the polymer template at high temperature were flexible and demonstrated a wrinkled surface (Fig. 1b). After sonication treatment, the TiO_2 nanomembrane was found to roll up into microscrolls with diameter of ~2 μm, and Fig. 1c demonstrates that the sonication also produced aggregation of TiO_2 microscrolls. Fig. 1d is the morphology of TiO_2 microscroll/graphene composite, and overlap between TiO_2 nanomembrane and graphene could be observed, suggesting possibly good contact between them. Fig. 1e is a large-area image of the TiO_2 microscroll/graphene composite on the electrode. A dense sensing layer consisted of the composite was observable. More details about the TiO_2 microscrolls could be observed in the enlarged image in Fig. 1f. One can see that the inner surface of the microscroll is very rough, consisting of small TiO_2 grains (see blue arrows). This porous structure was produced during ALD process, because the conformal coating well duplicated the rough surface of the original polymer template. According to our previous work [41], metal oxide nanomembranes deposited on polymer template via ALD process exhibit large surface area. In addition, it is worth noting that the microscroll with cylindrical geometry should promote three-dimensional diffusion of the ions, and both inner and outer surfaces can contact with the analyte in the solution at the same time, increasing the interaction area remarkably [13].

The structural properties of the samples were further investigated by Raman spectroscopy. Raman spectra of graphene, TiO_2 microscroll, and TiO_2 microscroll/graphene composite are shown in Fig. 1g. The Raman spectrum of graphene exhibits D and G peaks at 1353 and 1597 cm^{-1}, respectively. The D peak (inset of Fig. 1g) can be attributed to the stretching motion of sp^2 mode, which involves the inelastic and elastic scattering of an electron with, respectively, a phonon and defects [42,43], while the G peak corresponds to primary sp^2 and a doubly-degenerated phonon mode (E_{2g} symmetry) at the Brillouin zone [44]. The presence of TiO_2 E_g (147 cm^{-1}), B_{1g} (395 cm^{-1}), B_{1g} (522 cm^{-1}), and E_g (635 cm^{-1}) modes in TiO_2 microscroll and TiO_2 microscroll/graphene composite (Fig. 1g) indicates the crystal structure of TiO_2 nanomembrane is anatase [45]. The co-existence of both TiO_2 peaks and graphene peaks in the composite proved that both components exist in the sample.

3.2. Electrochemical characterization and optimization

EIS was also used to study the resistance and surface status of the sensing materials in our experiment. As shown in Fig. 2a, the impedance of the TiO_2 nanomembrane electrode was large (orange line in Fig. 2a), which is mainly due to the large resistivity of TiO_2. After the TiO_2 nanomembranes roll up to form TiO_2 microscrolls, the impedance decreased slightly (black line in Fig. 2a), due to the increased electrolyte/nanomembrane interface area. A significant impedance decrease was observed in TiO_2 microscroll/graphene composite (red line in Fig. 2a). This phenomenon proves that the graphene in the composite indeed facilitates fast electronic transporting which may improve the sensitivity of the sensing layer. The effect of pH of the buffer solutions on the electrochemical signal was also studied. In the experiment, the analyte solution including 1 mol L^{-1} Tris-HCl and 0.2 μmol L^{-1}DA was chosen as the substrate solution for the DPV test. As shown in Fig. 2b, the pH of the Tris-HCl solution was tuned in the range of 5.0–8.0 by adding 0.1 mol L^{-1} HCl. The experimental results demonstrate that with the increase of pH, the peak current (I_{pa}) increased gradually at the beginning, and decreased after the value reached the maximum. As shown in Fig. 2b, I_{pa} reached the maximum when the pH of the analyte solution was about 7.0. The PH value of ~7.0 favors the oxidation of dopamine, and therefore, the pH of 7.0 was chosen for further assay in our experiment. Similar pH dependent peak current behavior has also been reported in previous literature [28], and the detailed mechanism needs further investigation.

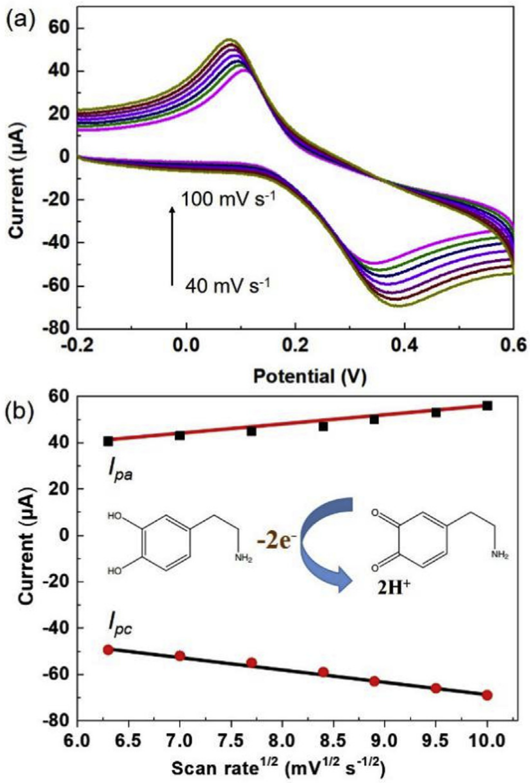

Fig. 3. a) CV curves of TiO_2 microscroll/graphene composite electrode in electrolyte containing 0.7 μmol L^{-1} DA and 1 mol L^{-1} Tris-HCl buffer solution. The scan rate is increased from 40 to 100 mV s^{-1} with a step of 10 mV s^{-1}. b) Peak currents (I_{pa} and I_{pc}) as a function of the scan rate, and the values are derived from (a). The blue squares and red spheres correspond to oxidation (I_{pa}) and reduction (I_{pc}) peak currents respectively. The inset schematically shows the DA oxidation process on the surface of electrode. (For interpretation of the references to colour in this figure legend, the reader is referred to the Web version of this article.)

3.3. Kinetics of TiO_2 microscroll/graphene electrochemical sensor

A scan rate study was performed to obtain information about the kinetic properties and the electrochemical behavior of the electrode. The electro-kinetics of DA oxidation at TiO_2 microscroll/graphene electrode was evaluated in an analyte solution including Tris-HCl (1 mol L^{-1}, pH 7.0) and DA (0.7 μmol L^{-1}) as a function of scan rate ranging from 40 to 100 mV s^{-1} (Fig. 3a). In the oxidation process, the carbon-oxygen single bond changed into carbon-oxygen double bond, and free electrons and H^+ were released in the process of oxidation. Quantitatively, the oxidation peak current (I_{pa}) and reduction peak current (I_{pc}) versus square root of scan rate ($v^{1/2}$) were plotted in Fig. 3b, and one can see that both I_{pa} and I_{pc} increased linearly with $v^{1/2}$. According to Andrieux et al. [46], the linear behavior indicates that the oxidation process of DA is controlled by diffusion and limited by the mass transport. For diffusion controlled redox processes [47], peak current I_p can be expressed as:

$$I_p = 0.496FSc_A D_A^{1/2}\left(\frac{Fv}{RT}\right)^{1/2} \tag{1}$$

where S is electrode surface area, c_A is bulk concentration of analyte solution, D_A is the diffusion coefficient of detected molecules, F is Faraday's constant, v is sweep rate, R is gas constant, and T is temperature. Thus, the measured current in the present experiment should be linearly proportional to $v^{1/2}$ (Fig. 3b). The underneath mechanism is that DA is oxidized into dopamine quinone (inset of Fig. 3b) under the stimulation of pulsed voltage. Based on the dependence of the peak current on the square root of the scan rates, the electrochemical behavior is considered to be diffusion-control, and the number of transferred electron is estimated to be ~1. In addition, the resultant composites exhibit high electroactive surface area of 0.031 cm^2. Large electrode surface area from porous TiO_2 nanomembrane leads to exposure of more active sites, which further enhances the electrochemical property.

3.4. Electrochemical behavior of TiO_2 microscroll/graphene senor

The electrochemical properties of the samples were specifically investigated by DPV tests. As shown in Fig. S1, TiO_2 microscroll/graphene composite (line iv) exhibits the largest peak current compared with TiO_2 nanomembrane (line i), TiO_2 microscroll (line ii), and graphene (line iii), indicating the best electrochemical property due to the synergy effects of self-rolled TiO_2 microscroll and conductive graphene. Due to very few catalytic active sites in graphene, TiO_2 nanomembrane, and TiO_2 microscrolls, they exhibit weak oxidation current signal. In addition, the TiO_2 nanomembrane electrode shows a broad oxidation peak with gentle slope because of the sluggish electrochemical response toward DA. The TiO_2 microscroll electrode shows a similar response behavior with a slightly increased current. One may note that the graphene electrode also has large oxidation current. However, the line shapes of the curves from graphene and microscroll/graphene composite electrodes are different, indicating a different electrochemical process. Due to the lack of active sites exposing, the electrochemical process occurring in the pure graphene is mainly controlled by the speed of electron transfer, while in the TiO_2 microscroll/graphene composite, diffusion process dominates the electrochemical reaction. As a result, different line shapes can be observed. The enhancement of the current of TiO_2 microscroll/graphene composite electrode is mainly ascribed to improved electron transfer between TiO_2 microscroll and graphene in the sensing layer. Owing to the conjugated π network plane of graphene, electrons can move among the conjugated π-π bonds. The corresponding electron transfer process significantly prompts the efficiency of oxidation reaction [48,49].

In order to study the responsivity of the sensor, the device was immersed in solutions with different DA concentrations for the DPV measurement. As shown in Fig. 4, the current increased with the increase of the DA concentration in the range of 0.06–90 μmol L^{-1}. The relationship between current (i.e., I_{pa}) and DA concentration (c) can be described by the equation: $I_{pa} = 13.78x + 17.87$ ($R^2 = 0.9973$), where $x = (ln\ c + 0.43)$. The detection limit (DL) of the current electrochemical sensor was also determined, and the value reached 4.25×10^{-9} mol L^{-1} (DL = $3\delta_b$/K), indicating high electrocatalytic performance of the microscroll/graphene composite. In addition, it is worth noting that the sensitivity of this sensor is higher compared with those of common DA sensors [50–52].

3.5. Selectivity, stability, and reproducibility of the sensor

The selectivity is a very important parameter to evaluate the performance of the sensor. The impact of interference was studied in the present investigation. K^+, Na^+, and Cl^- ions and glucose, with 1000 times higher concentration (i.e., 0.2 mmol L^{-1}), which were possible interferences in urine samples, showed no obvious influence on the peak current when they were mixed in a test solution containing 0.2 μmol L^{-1} DA (Fig. 5). In addition, the interference from structural analogues such as 0.2 mmol L^{-1} hydroquinone (HQ) and 0.2 mmol L^{-1} catechol was also investigated. Here, additional 0.2 μmol L^{-1} DA was also added and the increase of the current (~8 μA) is demonstrated in Fig. 5 as a reference. Considering the much lower concentration of the DA in the test solution, we should stress that the current microscroll/graphene DA sensor had very high selectivity.

The reproducibility of the sensor was evaluated by DPV testing in test solution containing 0.2 μmol L^{-1} DA. Here a sensor was tested for 5

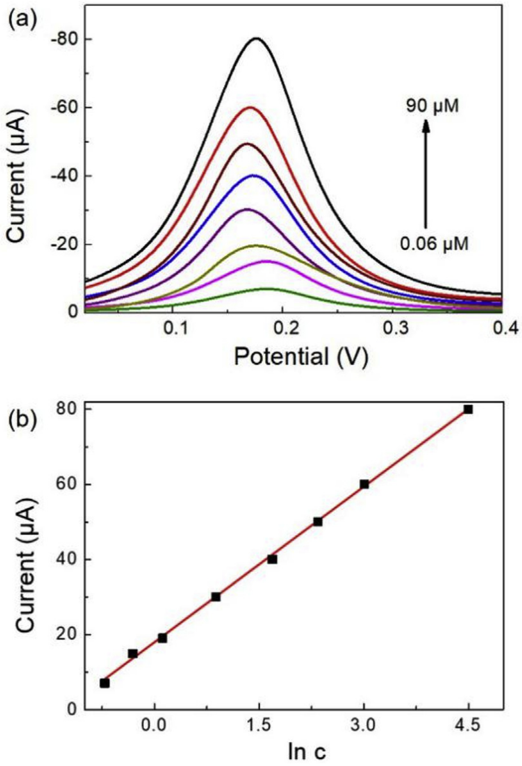

Fig. 4. a) DPV currents of TiO_2 microscroll/graphene sensor in test solutions with different DA concentrations ranging from 0.06 to 90 μmol L^{-1}. b) Experimental current (black squares) as a function of *ln c*. The red line is the fitting curve of the experimental data. (For interpretation of the references to colour in this figure legend, the reader is referred to the Web version of this article.)

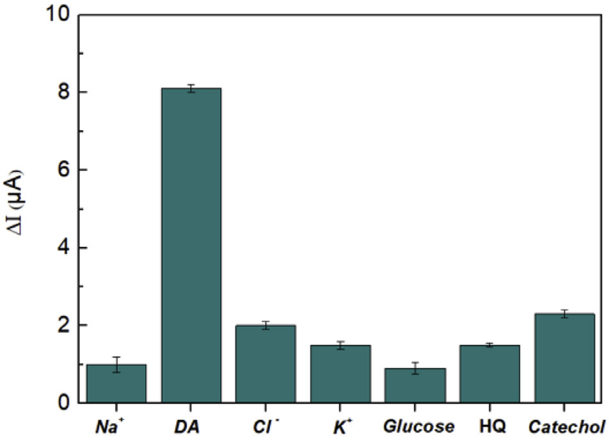

Fig. 5. Selectivity study of TiO_2 microscroll/graphene composite-based sensors toward 0.2 μmol L^{-1} of DA in Tris-HCl buffer solution.

times and the relative standard deviation (RSD) was 2.12%, while five different sensors prepared in the same way demonstrated a RSD of 3.45%. These results indicate that the sensor had good reproducibility. The stability was further evaluated by testing 0.2 μmol L^{-1} DA after certain period, and when not in use, the sensor was stored in refrigerator at 4 °C. The DPV curves of TiO_2 microscroll/graphene composite in 0.2 μmol L^{-1} of DA after storage of different days are shown in Fig. S2, and the deviations are calculated to be 0.4 μA (5 day), 0.2 μA (10 day), and 0.2 μA (30 day), respectively. Our experimental results demonstrate that the sensor is quite stable.

Table 1
The samples test results and recovery experiments with calibration method.

Sample	Added 10^{-6} mol/L	Total found 10^{-6} mol/L	RSD (n = 5) %	Recovery %
1	5.0	5.3	3.2	106
	10.0	9.8	1.8	98
2	5.0	4.7	2.8	94
	10.0	10.4	2.1	104

RSD of five independent measurements.

3.6. *Application of the composite sensor*

2.5 mL human urine was diluted to 100 mL with phosphate buffer at pH 7.0 to obtain the samples, and was analyzed by using our sensor device. The spiked samples with known amount of DA were added to urine sample to calculate the recovery. The determination results are shown in Table 1, with the recovery rate of 94.0–106.0% and RSD of < 4%, which proves that the sensor can be applied to the analysis of DA in urine samples.

4. Conclusion

In this work, microscroll/graphene composite has been fabricated with the help of ALD and sonication process, and then used as electrochemical sensor for DA detection. The composite provides large surface area and fast electron transfer path for DA oxidation under various conditions. The obtained sensor exhibits wide sensing linear range and low DL of 4.25 × 10^{-9} mol L^{-1}. The kinetic process of DA catalytic reaction on the electrode has been studied by using DPV, CV, and EIS characterizations. It can be noticed that the oxidation process of DA is controlled by diffusion and limited by the mass transport. For potential practical application, the current results demonstrate that the sensor can be applied to detect DA in urine. This work provides a new strategy for sensing DA in aqueous solution, and it may be extended to other neurotransmitters in the future.

Declaration of competing interest

The authors declare that they have no known competing financial interests or personal relationships that could have appeared to influence the work reported in this paper.

Acknowledgements

This work is supported by the National Natural Science Foundation of China (51961145108), Science and Technology Commission of Shanghai Municipality (17JC1401700, 19JC1415500, 19XD1400600).

Appendix A. Supplementary data

Supplementary data to this article can be found online at https://doi.org/10.1016/j.pnsc.2020.02.008.

References

[1] N.T.N. Phan, X.C. Li, A.G. Ewing, Nat. Rev. Chem. 16 (2017) 0048.
[2] M. Taleb, R. Ivanov, S. Bereznev, S.H. Kazemi, I. Hussainova, Microchim. Acta 184 (2017) 4603.
[3] J. Kim, A.S. Campbell, J. Wang, Talanta 177 (2018) 163.
[4] J.R. Anusha, B.C. Kim, K.H. Yu, Biosens. Bioelectron 142 (2019) 111511C. J. Raj https://www.sciencedirect.com/science/article/pii/S0956566319305901.
[5] S. Sharma, N. Singh, V. Tomar, R. Chandra, Biosens. Bioelectron. 107 (2018) 76.
[6] J.M. Moon, N. Thapliyal, K.K. Hussain, R.N. Goyal, Y.B. Shim, Biosens. Bioelectron. 102 (2018) 540.
[7] H. Beitollahi, M. Safaei, S. Tajik, Anal. Bioanal. Chem. Res. 6 (2019) 81.
[8] B.J. Sanghavi, O.S. Wolfbeis, T. Hirsch, N.S. Swami, Microchim. Acta 182 (2015) 1.
[9] Y.F. Mei, A.A. Solovev, S. Sanchez, O.G. Schmidt, Chem. Soc. Rev. 40 (2011) 2109.

[10] S. Xin, Y.G. Guo, L.J. Wan, Acc. Chem. Res. 45 (2012) 1759.
[11] Y.S. Hu, Y.G. Guo, R. Dominko, M. Gaberscek, J. Jamnik, J. Maier, Adv. Mater. 19 (2007) 1963.
[12] R. Samba, K. Fuchsberger, I. Matiychyn, S. Epple, L. Kiesel, A. Stett, W. Schuhmann, M. Stelzle, Electroanalysis 26 (2014) 548.
[13] H.X. Ji, X.L. Wu, L.Z. Fan, C. Krien, I. Fiering, Y.G. Guo, Y.F. Mei, O.G. Schmidt, Adv. Mater. 22 (2010) 4591.
[14] W. Huang, J.C. Zhou, P.J. Froeter, K. Walsh, S.Y. Liu, M.D. Kraman, M.Y. Li, J.A. Michaels, D.J. Sievers, S.B. Gong, X.L. Li, Nat. Electron. 1 (2018) 305.
[15] X.F. Wang, Y. Chen, O.G. Schmidt, C.L. Yan, Chem. Soc. Rev. 45 (2016) 1308.
[16] B.E.F. De Avila, W. Gao, E. Karshalev, L.F. Zhang, J. Wang, Acc. Chem. Res. 51 (2018) 1901.
[17] E. Topoglidis, C.J. Campbell, A.E.G. Cass, J.R. Durrant, Langmuir 17 (2001) 7899.
[18] J. Zhang, X. Yu, W. Guo, X.N. Mou, A.X. Li, H. Liu, Nanoscale 8 (2016) 9382.
[19] D. Gong, C.A. Grimes, O.K. Varghese, W.C. Hu, R.C. Singh, Z. Chen, E.C. Dickey, J. Mater. Res. 16 (2001) 3331.
[20] P. Hoyer, Langmuir 12 (1996) 1411.
[21] A.K.M. Kafi, G. Wu, A.C. Chen, Biosens. Bioelectron. 24 (2008) 566.
[22] X.D. Wang, Z.D. Li, J. Shi, Y.H. Yu, Chem. Rev. 114 (2014) 9346.
[23] X. Feng, K. Shankar, M. Paulose, C.A. Grimes, Angew. Chem. Int. Ed. 48 (2009) 8095.
[24] M. Iida, T. Sasaki, M. Watanabe, Chem. Mater. 10 (1998) 3780.
[25] J.C. Yu, L. Zhang, Z. Zheng, J.C. Zhao, Chem. Mater. 15 (2003) 2280.
[26] S. Cosnier, A. Senillou, M. Grätzel, P. Comte, N. Vlachopoulos, N.J. Renault, C.A. Martelet, J. Electroanal. Chem. 469 (1999) 176.
[27] S. Madhugiri, B. Sun, P.G. Smirniotis, J.P. Ferrarisa, J.K. Jr Balkus, Microporous Mesoporous Mater. 69 (2004) 77.
[28] C.L.L. Pham, S.L. Leong, F.E. Ali, V.B. Kenche, A.F. Hill, S.L. Gras, J. Mol. Biol. 387 (2009) 785.
[29] D.S.R. Josephine, K.J. Babu, K. Sethuraman, Microchim Acta 184 (2017) 781.
[30] K.S. Novoselov, A.K. Geim, S.V. Morozov, D. Jiang, Y. Zhang, S.V. Dubonos, I.V. Grigorieva1, A.A. Firsov, Science 306 (2004) 666.
[31] F. Schedin, A.K. Geim, S.V. Morozov, E.W. Hill, P. Blake, M.I. Katsnelson, K.S. Novoselov, Nat. Mater. 6 (2007) 652.
[32] J.C. Meyer, A.K. Geim, M.I. Katsnelson, K.S. Novoselov, T.J. Booth, S. Roth, Nature 446 (2007) 60.
[33] A.A. Grace, K.P. Divya, V. Dharuman, J.H. Hahn, Electrochim. Acta 302 (2019) 291.
[34] S. Arora, M.K.P. Kumar, C. Srivastava, Appl. Phys. A Mater. 125 (2019) 674.
[35] P. Li, B. Zhang, T.H. Cui, Sensor. Actuator. B Chem. 216 (2015) 337.
[36] D.Z. Zhang, H.Y. Chang, P. Li, R.H. Liu, Q.Z. Xue, Sensor. Actuator. B Chem. 225 (2016) 233.
[37] D.Z. Zhang, J.J. Liu, C.X. Jiang, P. Li, Y. Sun, Sensor. Actuator. B Chem. 245 (2017) 560.
[38] H. Chen, M.B. Müller, K.J. Gilmore, G.G. Wallace, D. Li, Adv. Mater. 20 (2008) 3557.
[39] Y. Fan, J.H. Liu, H.T. Lu, Q. Zhang, Colloids Surf. B Biointerfaces 85 (2011) 289.
[40] S.Q. Pan, Y.T. Zhao, G.S. Huang, J. Wang, S. Baunack, T. Gemming, M.L. Li, L.R. Zheng, O.G. Schmidt, Y.F. Mei, Nanotechnology 26 (2015) 364001.
[41] Y.T. Zhao, G.S. Huang, D.R. Wang, Y. Ma, Z. Fan, Z. Bao, J. Mater. Chem. 6 (2018) 22870.
[42] A.C. Ferrari, J. Robertson, J. Phys. Rev. B 61 (2000) 14095.
[43] A. Sanders, R.W. Bowman, L. Zhang, V. Turek, D.O. Sigle, A. Lombardi, L. Weller, J.J. Baumberga, Appl. Phys. Lett. 109 (2016) 153110.
[44] D. Naumenko, V. Snitka, B. Snopok, S. Arpiainen, H. Lipsanen, Nanotechnology 23 (2012) 465703.
[45] N.N. Dinh, N.T.T. Oanh, P.D. Long, M.C. Bernard, A. Hugot-Le Goff, Thin Solid Films423 (2003) 70.
[46] C.P. Andrieux, J.M. Saveant, J. Electroanal. Chem. Interfacial Electrochem. 93 (1978) 163.
[47] H. Jaegfeldt, T. Kuwana, G. Johansson, J. Am. Chem. Soc. 105 (1983) 1805.
[48] L. Yang, R.L. Zhang, B.H. Liu, J.P. Wang, S.H. Wang, M.Y. Han, Z.P. Zhang, Angew. Chem. Int. Ed. 53 (2014) 10109.
[49] J.T. Robinson, S.M. Tabakman, Y.Y. Liang, H.L. Wang, H.S. Casalongue, D. Vinh, H.J. Dai, J. Am. Chem. Soc. 133 (2011) 6825.
[50] X.J. Zhang, J.B. Zheng, Sensor. Actuator. B Chem. 290 (2019) 648.
[51] Z. Song, G. Sheng, Y.G. Cui, M.R. Li, Z.L. Song, C.F. Ding, X.L. Luo, Microchim. Acta 186 (2019) 220.
[52] Y.Y. Qian, C.A. Ma, S.P. Zhang, J.J. Gao, M.X. Liu, K.J. Xie, S. Wang, K. Sun, H.O. Song, Sensor. Actuator. B Chem. 255 (2018) 1655.